J Solid State Electrochem (2006) 10: 643–650
DOI 10.1007/s10008-006-0131-1

ORIGINAL PAPER

Xiong Yin · Catherine Choong · Liang Hong · Zhaolin Liu

Crafting $La_{0.2}Sr_{0.8}MnO_{3-\delta}$ membrane with dense surface from porous YSZ tube

Received: 14 December 2005 / Accepted: 28 December 2005 / Published online: 6 May 2006

Abstract This work reports a new design of asymmetric tubular oxygen-permeable ceramic membrane (OPCM) consisting of a porous Y_2O_3 stabilized ZrO_2 (YSZ) tube (with ~1 μm of pore diameters and 31% porosity) as the support and a gas-tight mixed conductive membrane. The membrane has an interlocking structure composed of a host matrix, Ag(Pd) alloy (9:1 by wt) doped perovskite-type $La_{0.2}Sr_{0.8}MnO_{3-\delta}$ (LSM80, 90wt%), and the embedded constituent, pristine LSM80. The Ag(Pd) alloy component promotes not only electronic conductivity and mechanical strength but also reduction of both porosity and pore sizes in the layer (~10-μm-thick) where it dopes. The porous structure in this layer could then be closed through a solution coating procedure by which ingress of an aqueous solution containing stoichiometric nitrate salts of La^{3+}, Mn^{3+}, and Sr^{2+} to the pore channels takes place first and the mixture of nitrate salts left after drying is subjected to pyrolysis to generate tri-metal oxides in situ. This is followed by calcinations at l,300 °C to consolidate the embedded trioxide and to cohere them with the Ag(Pd)-LSM80 host matrix. The structure formed is dubbed LSM80(S)-Ag(Pd)-LSM80, which was confirmed gas-tight by electron micrograph and N_2 permeation test. Finally, we assess the chemical compatibility between LSM80 and YSZ at the sintering temperature by X-ray diffraction and electrochemical impedance analysis. The oxygen permeation of the fabricated LSM80(S)-Ag(Pd)-LSM80-YSZ membrane is within the temperature range of 600 to 900 °C. The tests reveal good compatibility between the LSM80 and YSZ and a reasonably high oxygen permeation flux in association with this OPCM assembly.

Keywords Asymmetric ceramic membrane · Oxygen separation · LSM–YSZ assembly · Dip coating · Solution coating

X. Yin · C. Choong · L. Hong (✉)
Department of Chemical and Biomolecular Engineering,
National University of Singapore,
10 Kent Ridge Crescent 119260,
Singapore, Singapore
e-mail: chehongl@nus.edu.sg
Tel.: +65-67791936
Fax: +65-68745029

Z. Liu
Institute of Materials Research & Engineering,
3 Research Link 117602,
Singapore, Singapore

Introduction

Mixed ionic (O^{2-}) and electronic conductors (MIEC) were widely studied for oxygen separation from air in many industrial processes such as partial oxidation of methane (POM) [1–3] to generate syngas (mixture of H_2 and CO), solid oxygen fuel cells (SOFCs) [4–7], gas sensor [8, 9], and oxidation catalysts [10, 11]. To date, lots of candidate ceramic MIEC with different thermal expansion coefficients (TECs) and chemical stability were developed. Two comprehensive reviews by Julbe et al. [5] and Kharton et al. [6] conclude the recent development of the oxygen-permeable ceramics. It is generally considered that a higher oxygen ionic conductivity will result in lower chemical stability at reducing atmosphere (e.g., syngas and CH_4) because a fast oxygen mobility is originated from weak metal-oxygen chemical bonding, which in turn makes the metal(s) be easily reduced in the reducing atmosphere and at high temperatures.

For a POM reactor or an SOFC, an oxygen-permeable ceramic membrane (OPCM) is required to possess both high oxygen permeability and chemical stability in the reducing atmosphere and at the temperature that the conduction of oxygen ions in ceramic lattice needs. These two major features are crucial to real applications [12–14]. Meanwhile, the asymmetric configuration of OPCM in which a dense reactive membrane is coated on a porous support was the desired model in pursuit of both high oxygen permeability and membrane stability. Decreasing thickness of the reactive membrane to its characteristic width would enhance the oxygen permeability significantly [15]. It was also widely accepted that a thin

membrane could be kinetically favorable in maintaining the chemical stability of membrane at reducing environment because a limited bulk oxygen transport rate is responsible for the unwanted chemical reductions at the membrane surface [16–18].

Up to now, many studies have focused on the fabrication of planar asymmetric discs [13, 16, 19–23] by means of sputtering, spray coating, dip coating, slurry casting, or other techniques. Compared to asymmetric tubular ceramic membrane, planar structure is technically much easier to realize; however, the planar membranes would face limited application prospective in terms of having difficulties for scaling up and significant edge leakage effect [24]. Since Siemens Westinghouse's work to assemble a SOFC by laying a dense Y_2O_3 stabilized ZrO_2 (YSZ) oxygen electrolyte membrane, via the expensive electrochemical vapor deposition procedure, on a porous cathodic support [25], looking for cost-effective techniques to achieve the same goal was a challenge to the development of commercial OPCM. A method through multiple-sintering steps to form a dense ceramic layer on a porous support was developed [26] despite a high energy consuming process. The sol–gel coating technique is a low temperature process [27–30] with relatively low fabrication cost, but it is very difficult to be rid of crack formation in a coating layer during drying and burning treatment, especially when such a coating is developed on a tubular support.

This paper proposed a new type of wet chemistry method that combines dip coating and solution coating methods for the fabrication of an asymmetric OPCM. Perovskite-type $La_xSr_{1-x}MnO_{3-\delta}$ (LSM) was well known to be the porous cathode in conjunction with YSZ electrolyte in SOFCs because they have excellent chemical compatibility and rather close TECs [31–34]. LSM has a relatively high electronic conductivity but a low oxygen ionic conductivity while YSZ is almost a pure oxygen electrolyte. It was reported that the oxygen diffusivity of LSM can be significantly improved by forming a composite with YSZ and the composite has a higher effective oxygen surface exchange coefficient than either component [32]. An alternative design based on using these two materials was attempted in the following work in which the main technical progress achieved is the implantation of a dense LSM membrane on porous YSZ tube by means of a simple approach and the LSM membrane exhibits oxygen permeability at the level it should reach at the designated temperature point.

Materials and methods

Fabrication of the porous tubular YSZ support

The details about the preparation of a ceramic-polymer blend for the extrusion of ceramic tube were described in our previous work [35, 36]. Table 1 lists the recipe of YSZ-polymer blend for extrusion and, hence the green body of the extruded tube comprises 80wt% submicron YSZ powders. The extruded tube is placed in a Carbolite furnace and heated up (by 1 °C/min) to 400 °C and dwelled there for 1 h to burn off the polymers, and then the calcinations temperature is raised to 1,400 °C (by 2 °C/min) and held for 30 min to carry out sintering in the YSZ bulk. The sintered YSZ tube is porous (Fig. 1) with a porosity of about 31%.

Table 1 Chemical composition of the extrusion feed for making YSZ green tube

Components	Function	Content (wt%)
15mol% Y_2O_3 stabilized ZrO_2 (YSZ)	Ceramic	80
Hydroxyethyl cellulose (HEC) (MW: 90,000)	Pore-former	6
Polyethyleneglycol (PEG) (MW: 15,000)	Binder	12
Polyvinylpyrrolidone (PVP) (MW: 10,000)	Extrusion aid	2

Synthesis of fine LSM80 powders and formulation of colloidal suspensions

A Stoichiometric amounts of the three metal salts [$La(NO_3)_3{\cdot}6H_2O$, $C_4H_6O_4Mn{\cdot}4H_2O$, and $Sr(NO_3)_2$] are dissolved in an aqueous solution of $(NH_4)_4$-ethylenediamine-tetraacetic acid (EDTA, Aldrich) (pH 8~9) with 1:1 molar ratio of the metal ions to EDTA. Polyvinylalcohol (PVA) (5wt% of EDTA used) is then added and dissolved in the above solution. A gel-like substance is obtained after the solution became thick at 80 °C and the gel is thereafter subjected to burning at 350~400 °C to form a composite of the metal oxides. The powder is finally calcined at 900 °C for 1 h under air flow (100 l/h) in a Carbolite

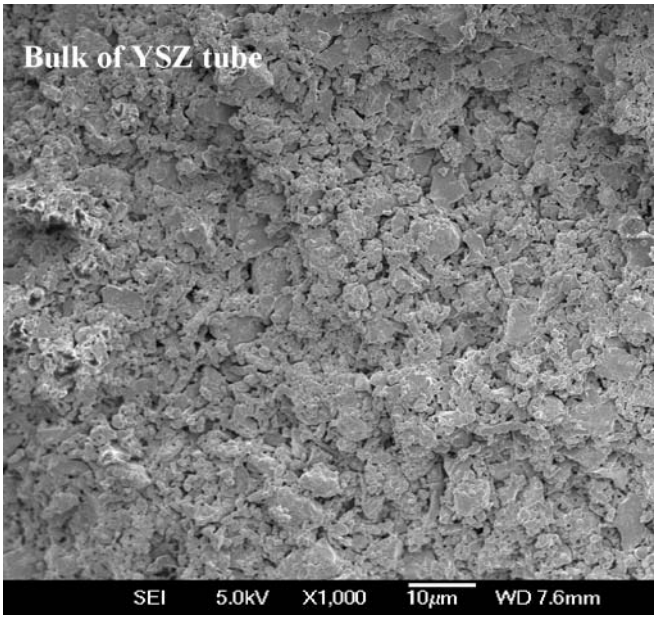

Fig. 1 The cross-sectional view of the sintered porous YSZ support

furnace to convert the oxide composite to the perovskite-type $La_{0.2}Sr_{0.8}MnO_{3-\delta}$ (LSM80). LSM80 powders are grounded and sieved through a 45-μm pore-sized sieve, which comprise primarily of submicron particles (Fig. 2). Details of the fabrication procedures were described in the previous papers [21, 22, 36, 37].

B A given amount of LSM80 fine powder (5.71 g) is suspended in an aqueous solution (1 l) containing $Pd(NO_3)_2$ (0.12 g), $AgNO_3$ (0.8 g), and PVA (0.71 g). After evaporating off the water at 80 °C, the residue is calcined at 350~400 °C to decompose the nitrates and calcined at 750 °C for 1 h and the product is a fine powder comprising Ag (Pd) alloy-coated LSM80 particles, i.e., Ag(Pd)-LSM80. According to the composition of feed, the dual phase Ag (Pd)-LSM80 contains approximately Ag (8.1wt%), Pd (0.9wt%), and LSM80 (91wt%).

C The colloidal suspension of either LSM80 or Ag(Pd)-LSM80 is formulated via the procedure described in [22]. The ink-like colloidal suspension consisting of 150 g/l LSM80 or Ag(Pd)-LSM80 powder, 6.25 g/l polyvinylbutyral (Butiva-79), 6 ml/l fish oil, 3 ml/l dibutyl phthalate, and 3 ml/l Span-80. A mixture of toluene and methylethylketone (v/v=1:1) was employed as the solvent. The resulting suspensions are ready to perform dip-coating.

Asymmetric tubular membrane preparation

A The porous YSZ tube is blocked at one end with epoxy resin, dipped into the LSM80 (or Ag(Pd)-LSM80) colloidal suspension for 1 min, and pulled out and this causes the formation of a thin LSM80 or Ag(Pd)-LSM80 powder-packing layer due to capillary force after drying under ambient condition. The coated tube is brought to burning at 400 °C for 1 h to eliminate organic additives and this is followed by calcinations at 1,300 °C for 3 h to sinter the coating layer; consequently, an asymmetric membrane, LSM80-YSZ or Ag(Pd)-LSM80-YSZ, is obtained.

B To completely close the surface pores existing in the above two membranes, the Ag(Pd)-LSM80-YSZ tube is coated by spraying an aqueous solution containing the three metal salts $La(NO_3)_3$ (0.2 M), $C_4H_6O_4Mn$ (1 M), and $Sr(NO_3)_2$ (0.8 M). After coating, the tube is first dried at 80 °C and subsequently heated at 350 °C for 1 h to decompose the trapped nitrates. This coat-dry-heat process is repeated five times and finally, the tube is calcined at 1,300 °C for 1 h to form a gas-tight LSM80(S)-Ag(Pd)-LSM80-YSZ membrane. However, it is impossible through this procedure to close pores in membrane LSM80-YSZ.

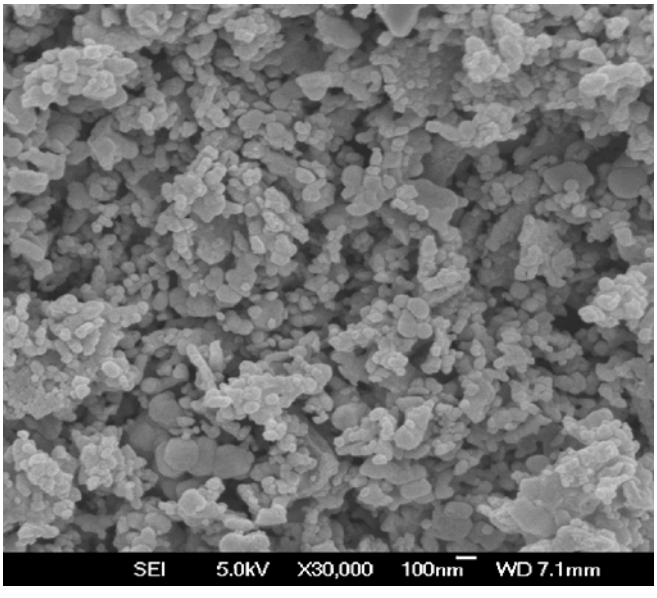

Fig. 2 Micrograph of the calcined LSM-80 fine powders

Structural and oxygen permeation assessments of the asymmetric tubular membrane

Figure 3 shows the schematic of the setup to check room temperature gas leakage (using N_2 as the sweeping gas) and oxygen permeation at high temperature (He as the sweeping gas) of the membrane. The details of the appraisal system were described in [30]. For carrying out the electrochemical impedance study, round disks, which are made of pristine YSZ or an equal-mass mixture of LSM80 and YSZ, are prepared by sintering the respective powder-packing pellets at 1,300 °C for 3 h. A minicell of Al_2O_3 is designed to fasten the disk together with two Ag electrodes via screwing the holder. This electrochemical cell is placed in a furnace and connected to the Solartron 1260 impedance analyzer for conducting impedance measurements (over the frequency from 500 Hz to 20 MHz) in the temperature range of 400~870 °C.

X-ray diffraction (XRD) patterns of the various specimens are established on a diffractometer (SHIMADZU XRD-6000) with CuK_α radiation (λ=1.54056 Å). The scanning speed is 2 °/min and the scanning angles cover from 20 to 80 °. Both surface and cross-sectional images of membrane are taken on a field emission scanning electron microscope (JSM-6700F, FESEM).

Results and discussion

From porous YSZ support to dense LSM80 surface requiring a transition layer

In contrast to the asymmetric electrolyte/cathode assembly in SOFC, the desired configuration for OPCM requirement

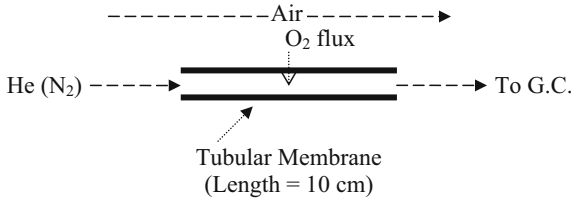

Fig. 3 Schematic of the setup for checking gas leakage and assessing oxygen permeation

is to attach a thin and dense MIEC membrane layer to a thick and porous YSZ support. Despite the fact that YSZ and LSM materials have similar TECs and good chemical compatibility, it is still not ready to realize a dense LSM membrane, which partially merges with the YSZ support underneath through a single step of coating on the porous YSZ support with a somewhat rough and porous surface (Fig. 4). Therefore, on such a surface, deposition of an LSM80 particle-packing by using the specially formulated colloidal dispersion (Section 2.1) would be an appropriate way to generate a consolidated membrane. However, the resulting LSM80 membrane through sintering is not yet dense and contains lots of pin holes as shown in Fig. 5a.

In the course of sintering, the defects with negative surface curvature are thermodynamically unstable and tend to grow [38]. The LSM80 fine powder, shown in Fig. 2, comprises particles from 10 to 200 nm, having the average particle diameter around 50 nm. It is unavoidable to form domains with different powder packing density as the agglomeration tendency is greater among smaller particles. Consequently, the formation of uneven domains is the root cause leading to the negative surface curvature pores, which would end up with pinholes after sintering at high temperature. Incorporating a metal alloy Ag(Pd) (Ag/Pd=9:1), which has a melting point well below the sintering temperatures of LSM80 and YSZ, into the ceramic phase by a content of 9wt% causes a decrease in the numbers of pinholes (Fig. 5b). It is supposed that Ag(Pd) alloy functions as a binder to help in the consolidation of LSM80 particles and as a pinhole filler after sintering. Unfortunately, the 9wt% alloy content is still not enough to eliminate all the pinholes and further increasing of the alloy content will cause coefficient of thermal expansion mismatch between the Ag(Pd)-LSM80 coating layer and the YSZ support.

Alternatively, plugging the surface pores through using the salt precursor as described in Section 2.3 could satisfactorily close pinholes in the Ag(Pd)-LSM80 membrane and realize a dense surface layer, LSM80(S)-Ag(Pd)-LSM80, as displayed in Fig. 5c. It is worthy to note that such a pore-plugging approach based on solution coating could be applicable only on the substrate with small pore sizes. The Ag(Pd)-LSM80 membrane is a transition layer that has a thickness of about 10 μm (Fig. 6) and offers a suitable porous structure for making this pore-closing approach viable. The energy-dispersive x-ray analysis of the outside surface of the LSM80(S)-Ag(Pd)-LSM80 membrane (Fig. 5c) at different locations showed that besides the elements of Ag, Pd, Zr, and Y, the membrane surface also has the La, Sr, and Mn elements with uniform local molar ratio close to 1:4:5 as designed.

The gas leakage tests of the porous YSZ tube, porous LSM80-YSZ membrane, porous Ag(Pd)-LSM80-YSZ membrane, and dense LSM80(S)-Ag(Pd)-LSM80-YSZ membrane are performed at room temperature (Section 2.4, Fig. 3). The O_2% by volume in the outlet gas stream decreases with increasing sweeping gas (N_2) flow rate (Fig. 7). This is considered to be a result of the enhancement of nitrogen fugacity, which brings about a reverse flow of N_2 toward airside. Furthermore, the O_2% is higher in the outlet stream from LSM80-YSZ membrane than that from Ag(Pd)-LSM80-YSZ membrane, showing the pore-reducing effect of the Ag(Pd) component in the membrane as stated above. The O_2% through the LSM80(S)-Ag(Pd)-LSM80-YSZ membrane is zero in the whole testing range, indicative of the success of the salt-precursor plugging approach, which leads to a gas-tight exterior side of Ag(Pd)-LSM80-YSZ membrane. In brief, gas leakage testing results are consistent with those based on the electron microscopy displayed in Fig. 5.

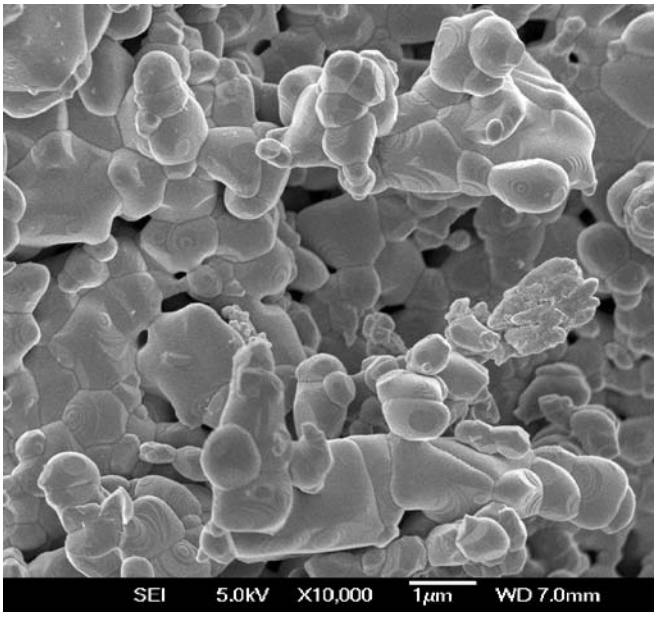

Fig. 4 The external surface morphology of the sintered YSZ tube

Chemical and electrochemical features of the LSM–YSZ interface

The chemical compatibility of LSM80 and YSZ was examined by sintering a pellet made of the two oxides (1:1 by wt) at 1,300 °C. Compared with the XRD patterns of the pristine LSM80 and YSZ, an extra peak (at 2θ=31.44°), although very weak, appears on the XRD pattern of the sintered pellet (Fig. 8). This peak, belonging to neither perovskite LSM80 nor cubic YSZ, is therefore attributed to a minor phase derived from the interfacial reaction between LSM80 and YSZ at the calcination temperature. The chemical compatibility between the LSM with YSZ was extensively investigated [39–42] and it was widely acknowledged that at the LSM–YSZ interface, the insulating pyrochlore-type $La_2Zr_2O_7$ (LZO) or perovskite-type $SrZrO_3$ (SZO) layer is formed at high sintering temperatures (≥1,100 °C) due to the relatively fast diffusion rate of La^{3+} or Sr^{2+} into the YSZ lattice. Sahu et al. [43], however, discovered that neither LZO nor SZO was found at the LSM–YSZ interface even when sintering at 1,400 °C for 6 h. This discrepancy is likely due to

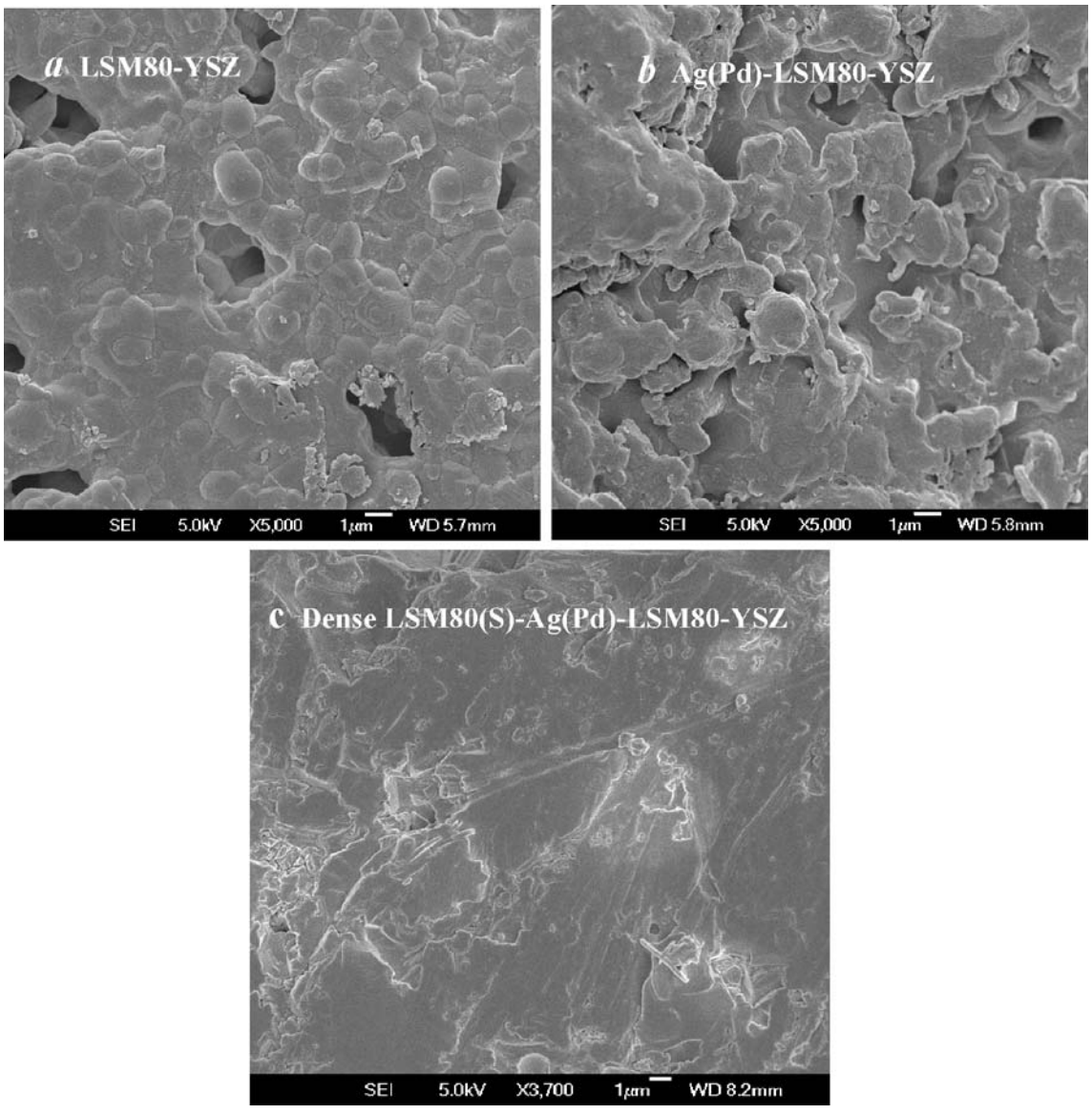

Fig. 5 The surface morphologies of the three membranes as indicated

different LSM compositions and the influence of the preparation methods. Because the diffusion of La^{3+} or Sr^{2+} into YSZ phase to form insulating LZO or SZO phase is driven by the chemical potentials of La^{3+} and Sr^{2+} at the LSM–YSZ interface, a homogeneous LSM composition should favor lowering down such diffusion tendency and similarly, a high Sr doping extent should favor the formation of SZO.

The experimental impedance spectra (EIS) of the pristine YSZ and YSZ-LSM80 (1:1 wt) pellets (obtained from sintering at 1,300 °C) are shown in Fig. 9a,b in which the spectra are expressed by Nyquist diagram, i.e., imaginary part (Z'') is plotted against real part of the impedance (Z'). The Nyquist plots of YSZ are approximately interpreted by an equivalent circuit as shown in Fig. 10a [44–46]. R_o is the sum of ohmic resistors due to electric connection including electrode ohmic resistance and contact resistance at interfaces. The high frequency impedance (f>0.01 MHz) is attributed to the resistance (R_e) and constant phase element (Q_e) of the YSZ electrolyte; while the low frequency regime of the Nyquist plot is related to the electron transfer at the electrode (R_{ct} and Q_{dl}). The electrical conductivity of the YSZ-LSM80 composite (Fig. 9b) is much higher than that of the pure YSZ. The equivalent circuits as shown in Fig. 10b is used to explain the EIS of YSZ-LSM80 composite where L is the inductance that is taken into account because of the existence of magnetic Mn^{3+} ion, R_s the overall ohmic resistance [47, 48] including the electrolyte resistance and electric connection resistance and could be determined by the first intercept of the "arc" with the real axis (Z'), while R_p and Q_p are the electrochemical polarization resistance and its corresponding constant phase element, respectively, and R_p could be determined from the second intercept (Fig. 9b). Compared with YSZ, LSM80-YSZ displays a distorted Nyquist plot due to the occurrence of electronic

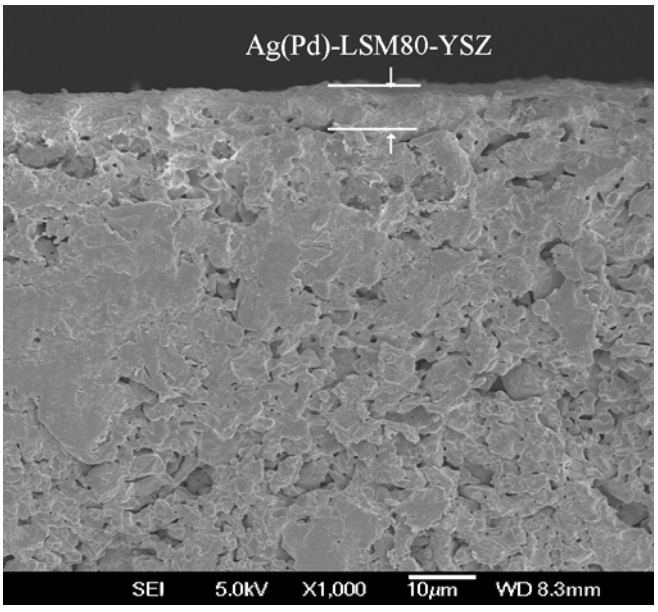

Fig. 6 The cross-sectional view of the Ag(Pd)-LSM80-YSZ membrane

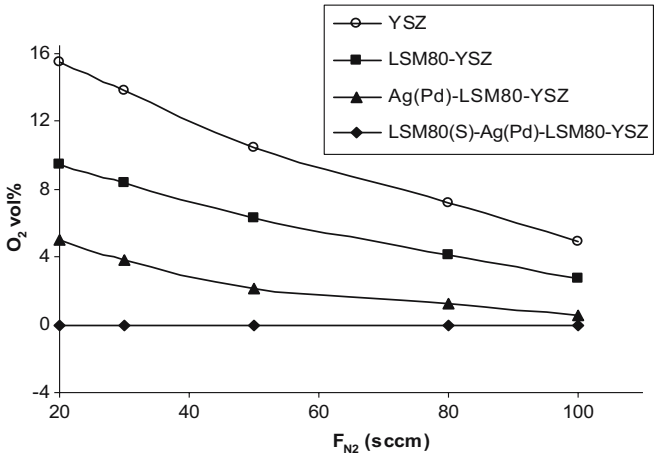

Fig. 7 The air leakage extents through different membranes with the change of sweeping gas flow rate at room temperature

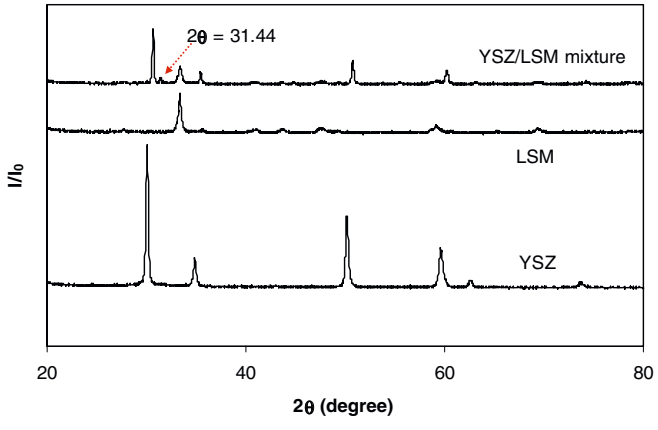

Fig. 8 XRDs of the ceramic pellet (pure YSZ, pure LSM80, and 1:1 wt mixture of LSM80 and YSZ) after calcinations at 1,300 °C for 3 h

conduction across the continuous LSM80 phase in the testing desk. This can also be evidenced by the weak response of its impedance to the increasing of temperature showed in Fig. 9b. In contrast to this, the impedance of YSZ (e.g., R_s+R_p value) shows an apparent temperature-dependency due to its ionic conduction nature. As a reference, the pristine LSM80 also manifests very similar R_s+R_p values with increasing of temperature (Fig. 9c). It is important to note that LSM80-YSZ and LSM80 possess very similar R_s+R_p values at all the temperature points examined, which implies that a tiny occurrence of the insulating phases (e.g., LZO or SZO) at the interface between LSM80 and YSZ affects very little the charge transfer through the LSM80 phase.

Figure 11 shows the temperature effect on the charge transfer in the bulk of electrolyte and at the electrode-ceramic interface, respectively. YSZ displays as expected the typical temperature-driven solid ionic conduction trend, but LSM80 is prevailed by its electronic conducting behavior that shields the ionic conduction so as the R_s of LSM80 undergoes basically no reduction with increasing temperature. For YSZ-LSM80 mixture, the ionic conduction component in both of its bulk conduction (R_s) and the charge transfer at electrode (R_p) increases with increasing temperature, and the trend of the later one is clearer than the former one. This result states that a tiny occurrence of the insulating phases (e.g., LZO or SZO) at the interface between LSM80 and YSZ also does not bar ion transfer though the YSZ phase. In the tubular membrane, LSM80 (S)-Ag(Pd)-LSM80-YSZ, the interface between LSM80 and YSZ has similar structure and properties to the YSZ-LSM80 mixture. The separation of oxygen from air through the tubular membrane was carried out in the temperature range from 600 to 900 °C (Fig. 12). The oxygen permeation flux experiences a big increase when the separation temperature is raised from 800 to 900 °C. According to the above electrochemical impedance analysis, it is suggested that the transfer of O^{2-} ions through LSM80 is a rate-determining step and a useful oxygen flux could be achieved only when the operation temperature hits 900 °C.

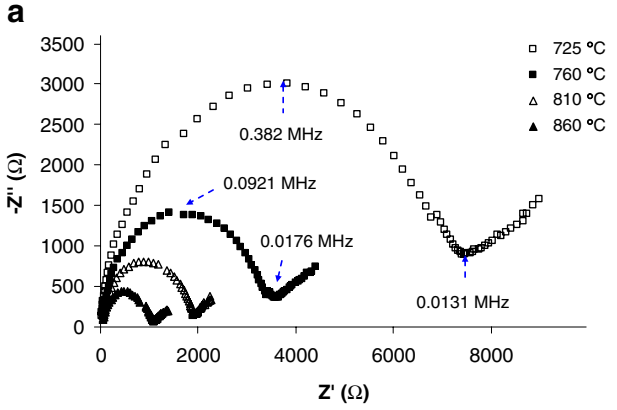

Fig. 9 Nyquist diagrams of **a** YSZ, **b** 1:1 wt mixture of LSM80 and YSZ, and **c** pure LSM80 at different measurement temperatures

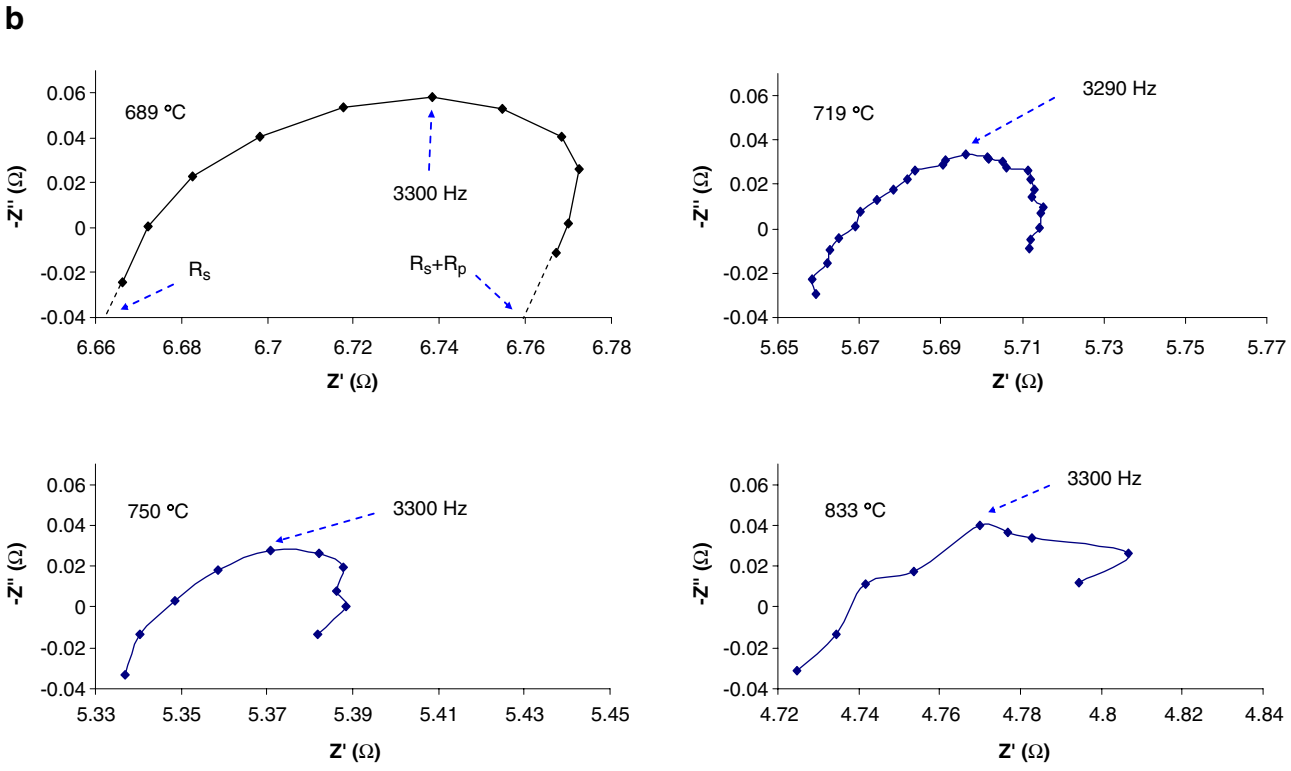

Fig. 9 (continued)

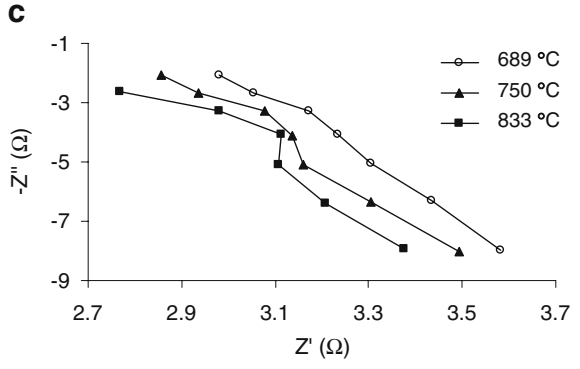

Fig. 9 (continued)

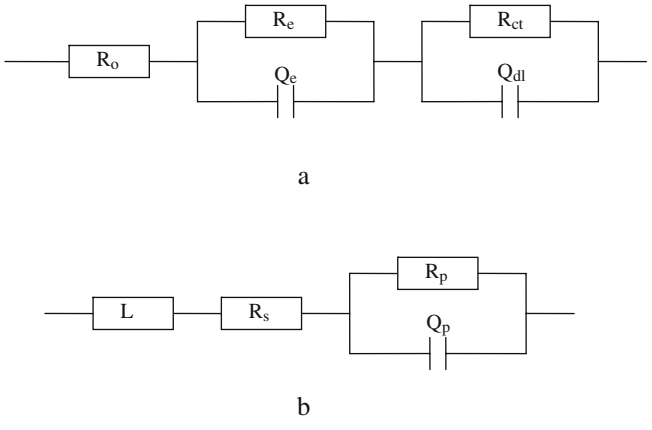

Fig. 10 Equivalent circuit models for describing the EIS of **a** YSZ and **b** 1:1 wt mixture of LSM80 and YSZ

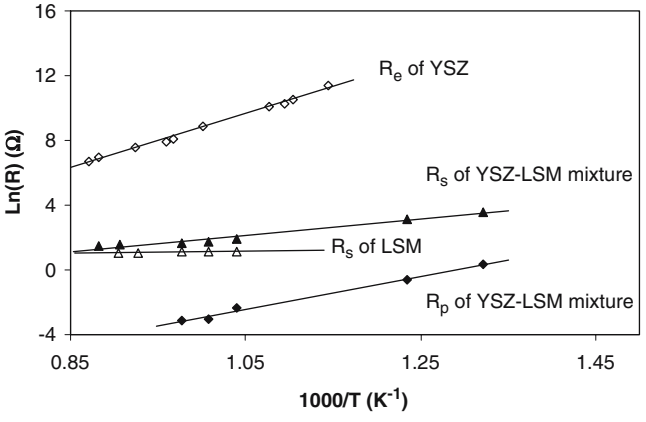

Fig. 11 The temperature-dependent charge transfer behaviors of YSZ, LSM80, and their composite

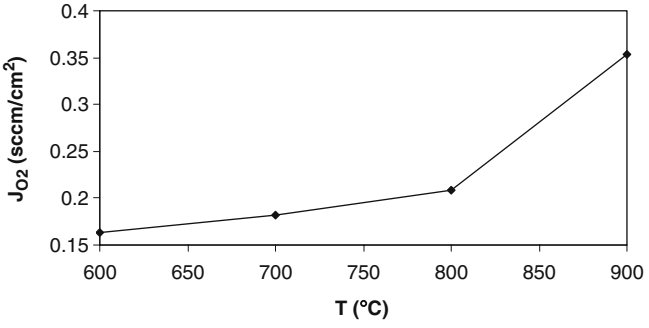

Fig. 12 The experimental oxygen permeation flux through the tubular asymmetric membrane, LSM80(S)-Ag(Pd)-LSM80-YSZ, at different temperatures and 1 bar in both feeding and purging sides

Conclusions

In this paper, a porous YSZ tube with a mean pore diameter around 1 μm and porosity of 31% was made through extrusion and sintering at 1,400 °C for 30 min. The target of this work is the fabrication of an asymmetric oxygen electrolyte membrane, LSM80-YSZ. To achieve the gas-tight state in the reactive LSM-80 layer, two methods were employed, which are, firstly, implementation of a dual phase metal-ceramic composite coating, Ag(Pd)-LSM80, and secondly, plugging surface pores of the coating layer by the salt-precursor approach. The presence of Ag(Pd) (ratio 9:1) alloy (9wt%) in the LSM80 phase reduces its porous feature. This is essential to assure success of the subsequent pore-closing step. The chemical compatibility and charge transport behavior at the interface between LSM80 and YSZ were investigated. The analysis results show that the occurrence of minor interfacial species generated from sintering the two oxides at 1,300 °C does not affect the oxygen ionic conductivity at the interface. The oxygen permeation of the asymmetric LSM80(S)-Ag (Pd)-LSM80-YSZ membrane gains an apparent increase when operation temperature is raised from 800 to 900 °C, reaching to 0.35 sccm/cm^2.

References

1. Tong J, Yang W, Cai R, Zhu B, Lin L (2002) Catal Letters 78:129
2. Tablet C, Grubert G, Wang H, Schiestel T, Schroeder M, Langanke B, Caro J (2005) Catal Today 104:126
3. Gu X, Jin W, Chen C, Xu N, Shi J, Ma YH (2002) AIChE J 48:2051
4. Sin A, Kopnin E, Dubitsky Y, Zaopo A, Aricò AS, Gullo LR, La Rosa D, Antonucci V (2005) J Power Sources 145:68
5. Julbe A, Farrusseng D, Guizard C (2005) Catal Today 104:102
6. Kharton VV, Marques FMB, Atkinson A (2004) Solid State Ion 174:135
7. Xia C, Liu M (2002) Solid State Ion 152–153:423
8. Bhatt HD, Vedula R, Desu SB, Fralick GC (1999) Thin Solid Films 350:249
9. Pollak C, Reichmann K, Hutter H (2002) Surf Coat Technol 150:119
10. Kim BJ, Lee J, Yoo JB (1999) Thin Solid Films 341:13
11. Kucharczyk B, Tylus W (2004) Catal Today 90:121
12. Figueiredo FM, Kharton VV, Viskup AP, Frade JR (2004) J Membr Sci 236:73
13. Armstrong T, Prado F, Manthiram A (2001) Solid State Ion 140:89
14. Shao Z, Yang W, Cong Y, Dong H, Tong J, Xiong G (2000) J Membr Sci 172:177
15. Bouwmeester HJM, Burggraaf AJ (1997) Dense ceramic membranes for oxygen separation. In: Gellings PJ, Bouwmeester HJM (eds) The CRC handbook of solid state electrochemistry. CRC Press, Boca Raton, FL, pp 481–553
16. Liu M, Wang D (1995) J Mater Res 10:3210
17. Balachandran U, Dusek JT, Sweeney SM, Poeppel RB, Mieville RL, Maiya PS, Kleefisch MS, Pei S, Kobylinski TS, Udovich CA, Bose AC (1995) Am Ceram Soc Bull 74:71
18. Mitchell BJ, Rogan RC, Richardson JW Jr, Ma B, Balachandran U (2002) Solid State Ion 146:313
19. Jin W, Li S, Huang P, Xu N, Shi J (2001) J Membr Sci 185:237
20. Xia C, Ward TL, Atanasova P, Schwartz RW (1998) J Mater Res 13:173
21. Liu Y, Hong L (2003) J Membr Sci 224:137
22. Hong L, Chua W (2002) J Membr Sci 198:95
23. Middleton H, Diethelm S, Ihringer R, Larrain D, Sfeir J, Herle JV (2004) J Eur Ceram Soc 24:1083
24. Lee TH, Yang YL, Jacobson AJ, Abeles B, Zhou M (1997) Solid State Ion 100:77
25. Feduska W, Isenberg AO (1983) J Power Sources 10:89
26. Ritchie JT, Richardson JT, Dan Luss (2001) AIChE J 47:2092
27. Yang J, Jianbin L (2005) Sens Actuators A 121:103
28. Wang ZJ, Kokawa H, Maeda R (2005) Acta Mater 53:593
29. Zelinski BJJ, Uhlmann DR (1984) J Phys Chem Solids 45:1069
30. Savaniu C, Irvine JTS (2002) Solid State Ion 150:295
31. Wandekar RV, Wani BN, Bharadwaj SR (2005) Mater Lett 59:2799
32. Ji Y, Kilner JA, Carolan MF (2005) Solid State Ion 176:937
33. Jiang SP (2003) J Power Sources 124:390
34. Tikhonovich VN, Kharton VV, Naumovich EN, Savitsky AA (1998) Solid State Ion 106:197
35. Yin X, Hong L, Liu ZL (2005) J Eur Ceram Soc 25:3097
36. Yin X, Hong L, Liu ZL (2005) J Membr Sci 268:2
37. Hong L, Guo F, Lin J (1999) Mater Res Bull 34:1943
38. Chiang Y-M, Birnie III DP, Kingery WD (1997) Physical ceramics: principles for ceramic science and engineering. Wiley, p 409
39. Barbucci A, Carpanese P, Cerisola G, Viviani M (2005) Solid State Ion 176:1753
40. Yang CCT, Wei WCJ, Andreas R (2003) Mater Chem Phys 81:134
41. Brant MC, Dessemond L (2000) Solid State Ion 138:1
42. Mitterdorfer A, Gauckler LJ (1998) Solid State Ion 111:185
43. Sahu AK, Ghosh A, Suri AK, Sengupta P, Bhanumurthy K (2004) Mater Lett 58:3332
44. Mitterdorfer A, Gauckler LJ (1999) Solid State Ion 117:203
45. Zhang WF, Schmidt-Zhang P, Guth U (2004) Solid State Ion 169:121
46. Jayaraj B, Desai VH, Lee CK, Sohn YH (2004) Mater Sci Eng A 372:278
47. JØrgensen MJ, Primdahl S, Mogensen M (1999) Electrochim Acta 44:4195
48. Leng YJ, Chan SH, Khor KA, Jiang SP (2004) Int J Hydrogen Energy 29:1025